From micro to macro: Physical-chemical characterization of wheat starch-based films modified with PEG200, sodium citrate, or citric acid

Veronica Ciaramitaro [a], Elena Piacenza [a,*], Paolo Lo Meo [a,*], Calogero Librici [b], Martina M. Calvino [c], Pellegrino Conte [b], Giuseppe Lazzara [c], Delia F. Chillura Martino [a]

[a] Department of Biological, Chemical, and Pharmaceutical Sciences and Technology (STEBICEF), Università degli Studi di Palermo, Viale delle Scienze pad. 17, 90128 Palermo, Italy
[b] Department of Agricultural, Food and Forest Sciences, Università degli Studi di Palermo, Viale delle Scienze pad. 4, Palermo, Italy
[c] Department of Physics and Chemistry - Emilio Segrè, Università degli Studi di Palermo, Viale delle Scienze pad. 17, Palermo, Italy

ABSTRACT

Needing to extend the shelf-life of packaged food and the evolving consumer demands led researchers to seek innovative, eco-friendly, and biocompatible packaging solutions. Starch is among the most promising natural and renewable alternatives to non-degradable plastics. Here, we deeply study the structural features of starch films modified by adding citric acid (CA) or sodium citrate (SC) as a cross-linker and polyethylene glycol 200 (PEG200) as a plasticizer and obtained through solvent casting. The substances' influence on starch films was evaluated through Attenuated Total Reflection Fourier Transform Infrared (ATR-FTIR) and Solid-state Nuclear Magnetic Resonance (ss-NMR) spectroscopies. Films' macroscopic properties, such as swelling index, solubility, thermo-mechanical features, and moisture absorption, were also assessed to foresee potential applications. Proper amounts of CA, CS, and PEG200 improve film properties and inhibit starch chains' retrogradation and recrystallization. Besides, the chemical neighbourhood of nuclei observed through ss-NMR significantly changed alongside the polymer chains' mobility. The latter result indicates a different polymer chain structural organization that could justify the film's higher resistance to thermal degradation and elongation at the break. This methodological approach is effective in predicting the macroscopic behaviour of a polymeric material and could be helpful for the application of such products in food preservation.

1. Introduction

Plastics have reached almost all areas of human lives, finding applications in various industries, such as the packaging industry, which accounts for nearly 40 % of global plastic production [1]. Plastic packaging is currently designed for a single-use or has a short service life, becoming a waste after consumption. Besides, the lack of information and awareness about its side effects, use, misuse, and waste disposal has turned the Earth into a plastic planet [2].

The food industry has invested heavily in response to environmental and market requirements, alongside wellness programs. The hustle and bustle of everyday life have greatly favoured the consumption of ready-to-eat fresh fruits or vegetables that have already been washed, cut, and packaged. To date, non-renewable raw materials destined for depletion are the principal materials used for food packaging. Therefore,

researchers are looking for new, cheap, alternative plastics with good properties based on renewable and natural raw materials, such as polysaccharides [3]. Among them, starch is one of the most promising alternatives to non-degradable plastics because it is an abundant, inexpensive, biodegradable, and edible material [4] that can find significant applications in bio-based packaging. Starch is composed of two glucose polymers, amylose [a linear polymer composed of $\alpha(1 \rightarrow 4)$ linked anhydrous-glucose residues, typically reported to have a molar mass of ca 10^5–10^6 g mol^{-1}] and amylopectin (a highly branched polymer consisting of short chains of $\alpha(1 \rightarrow 4)$ linked anhydrous-glucose residues, interspersed with 5–6 % branch points of $\alpha(1 \rightarrow 6)$ linkages, with a molecular weight perhaps as high as 10^7–10^9 g mol^{-1}) [5]. These two polymers form a complex semi-crystalline granular arrangement based on aggregates of double helices bounding adjacent branches of amylopectin molecules. Moreover, starch's amylose/amylopectin ratio

influences its physical-chemical properties, such as crystalline structure, viscosity, gel-formation capacity, shear-resistance ability, and water interaction, alongside those of starch films [6,7]. Specifically, films made from wheat starch - that holds an intermediate amount of amylose (ca. 25 %) than other starches - showed low wetting properties and good surface hydrophobicity, intermediate transparency, hydration (water solubility and swelling index) and barrier (water vapor and oxygen permeability) properties, and good tensile strength [8–11].

Regardless of the promising physical-chemical features of starch, this polymer has substantial drawbacks that have limited its use in packaging. For instance, the ratio of crystalline-to-amorphous material in the native starch varies greatly depending on the botanical origin of the biopolymer [12]. The massive inter- and intra-molecular interactions make starch it very brittle [13], and starch films are hydrophilic and generally feature low mechanical strength. Various options are available to overcome these hindrances and improve the properties of starch films. Adding cross-linkers and plasticizers to starch can improve film stability, flexibility, and extensibility and reduce its brittleness [14]. Specifically, cross-linking agents, such as citric acid (CA), sodium citrate (SC), and choline dihydrogen citrate salt, can improve tensile strength, thermal stability and decrease the dissolution of starch films in water [15–17]. A plasticizer is a substance added to synthetic or natural polymers to reduce brittleness by promoting plasticity and flexibility [18]. Plasticizers in appropriate proportions can also promote the stability of starch film and efficiently hamper recrystallization or retrogradation [19]. An ideal plasticizer should (*i*) reduce intermolecular strengths and moisture absorption, (*ii*) increase starch chain mobility, and (*iii*) be compatible with the biopolymer [14]. Currently, the most used starch plasticizers are small molecules with polar functional groups, such as —OH [20], —COOH [21], and —NH$_2$ [22]. No single plasticizer can meet all the required criteria, yet the cooperation of several plasticizing agents and their interaction with cross-linking agents can optimize the poor properties of starch films. In this regard, CA and polyethylene glycol (PEG) can be a promising combination, as they are both non-toxic and inexpensive [23–30]. CA-modified starch shows superior barrier properties and moisture resistance [28], whereas PEG plasticizer efficiency is inversely related to its molecular weight [23–25]. Specifically, PEG with a molecular weight >300 g mol^{-1} cannot plasticize starch by melt processing [31]. Moreover, PEG can prevent starch retrogradation to some extent. Although several reports focused on using CA alone or combined with diverse plasticizers to improve the quality of starch-based films, only a few studies explore the possibility of using polycarboxylates such as SC for the same purpose. Specifically, according to Zhang et al. [16], the combination of SC (20 wt%) and PEG200 (5 wt%) confers low crystallinity, low humidity sensitivity, and high resistance to elongation at the break to the starch film.

Based on the above considerations, we explored the cross-linking of the starch film (S) by CA and SC and the effect of PEG200 as a plasticizing agent. Starch was modified with either citric acid/PEG200 mixtures at various weight ratios or an SC/PEG200 mixture at a 4:1 weight ratio (i.e., the optimal reported in [16]). The comparison between structural changes and physical and thermal-mechanical properties of starch-based films and the non-modified one highlighted that CA, SC, and PEG200 improved the film quality, which can be relevant for food packaging development and application. Therefore, the present work aims to verify if a deep investigation of the microscopical features of a polymeric material can allow for rationalizing its macroscopic properties. Besides, the results of this study may help the translation of starch-based films from benchtop research to application in food preservation or other related fields.

2. Experimental section

2.1. Materials

Commercial wheat starch (S) was obtained from Paneangeli Cameo

S.p.A. Polyethylene glycol 200 (PEG200), tribasic sodium citrate dihydrate (SC, >99 %), citric acid monohydrate (CA, 98 %), glycerol (99.5 %), and sodium hydroxide (NaOH) were purchased from SIGMA Aldrich. Demineralized water (conductivity <10 μS/cm) was used in all experiments.

2.2. Preparation of starch-based films

Starch-containing dispersions (Table 1) were obtained by dissolving 16 g of starch into 380 g of water. Dispersions were then stirred at 150 rpm, heated at 95.0 ± 0.5 °C for 1 h, and then cooled to room temperature. Aliquots (20 ml) were poured into Petri dishes (80 mm diameter). Starch-based films were subsequently obtained through solvent casting at room temperature for 72 h.

The pH value of S_CA_PEG200 ternary dispersions was adjusted to 3.5 by adding appropriate amounts of a 10 M NaOH solution.

2.3. Attenuated total reflection - Fourier transform infrared spectroscopy (ATR-FTIR)

ATR-FTIR spectra were acquired through a VERTEX 70 V Bruker spectrophotometer equipped with a Platinum ATR unit with diamond crystal (η = 2.4) operating at 2 hPa in the spectral range between 4000 and 500 cm^{-1}, a spectral resolution of 2 cm^{-1}, and 200 scans. In all spectra, a baseline correction of scattering was made, and the 2000–2200 cm^{-1} range shows the characteristic auto-absorption feature of the diamond crystal. Data analysis was performed using the OPUS 7.5® software. ATR-FTIR spectra were subjected to a spectral deconvolution by non-linear least-squares fitting in the 1180–880 cm^{-1} region (Figs. S1–S4) using OriginPro software.

2.4. Solid-state NMR spectroscopy (ss-NMR)

The ^{13}C cross polarization-magic angle spinning nuclear magnetic resonance (^{13}C[^{1}H]CPMAS NMR) spectra of the prepared films (50 mg) were acquired at room temperature using a Bruker Avance II 400 MHz (9.4 T) spectrometer following the conditions described by Piacenza and colleagues [32].

2.5. NMR relaxometry

Two complementary NMR relaxometry approaches based on the longitudinal (spin-lattice) relaxation rates were used for characterizing starch-based films. The dynamics of the glucose subunit backbone was addressed by determining the T$_{1\rho}$(C) values for the cumulative signal at 75 ppm relevant to the C2, C3, and C5 of the glucose units. The carbon spin-lattice relaxation times in the rotating frame T$_{1\rho}$(C) were determined with the variable spin lock (VSL) pulse sequence [33] using delay times ranging from 0.4 to 30 ms and a contact time of 1.5 ms. The latter

Table 1
Composition of starch-containing dispersions.

Film acronym	Quantity of cross-linking and/or plasticizing agent added to starch-containing dispersions
Binary dispersions	
S_PEG200	4 g of PEG200 (25 % of the total polymer mass)
S_SC	4 g of sodium citrate (25 % of the total polymer mass)
S_CA	4 g of citric acid (25 % of the total polymer mass)
Ternary dispersions	
S_SC_PEG200	3.2 g of sodium citrate (20 % of the total polymer mass) and 0.8 g of PEG200 (5 % of the total polymer mass), weight ratio of 4:1.
S_CA_PEG200	3.2 g of citric acid (20 % of the total polymer mass) and an amount of PEG200 such that the CA/PEG200 ratio was 4, 2, 1, 0, 5, 0, 25. The abbreviations of these dispersions were CA4P1, CA2P1, CA1P1, CA1P2, CA1P4, respectively.

was chosen after the application of a variable contact time experiment according to references [34,35]. A spinning speed of 6 kHz was applied to ensure the removal of all the spinning side bands. $^{13}C[^{1}H]$CPMAS NMR spectra were processed by calculating the integral of the most intense peak, corresponding to the carbons of the glycosidic unit indicated in spectra as C2-3-5. The area values obtained are plotted as a function of contact time (Fig. S5), and data were subjected to regression analysis according to a simple first-order model.

The overall dynamics of the systems were assessed through the Fast-Field-Cycling (FFC) technique applied to the ^{1}H magnetization signal. The ^{1}H relaxation rates ($R_1 = T_1^{-1}$) were evaluated at different magnetic field values in the Larmor frequency (ν_L) range of 0.01–10 MHz, using a Stelar SmartRace apparatus. The obtained NMRD dispersion curves (i.e., the R_1 versus ν_L plots) were subjected to a Monte Carlo heuristic analysis procedure recently proposed by Landi and colleagues [36] (Supplementary material) to identify the main dynamic domains of the system [37].

2.6. X-ray diffraction (XRD) of starch-based films

XRD patterns of starch-based films were recorded with a RIGAKU D-MAX 25600 HK instrument. Analyses were performed in the 2-theta range from 5° to 30° using a copper Kα radiation (λ = 1.54 Å; setup conditions: tube voltage of 40 kV, current 40 mA, 0.02°/s). XRD patterns and the degree of crystallinity (DC) were analysed and calculated using Match! 3 software.

2.7. Thermogravimetric analysis of starch-based films

Thermogravimetric experiments were performed using a Q5000 IR apparatus (TA Instruments) in an inert atmosphere by heating the sample from room temperature to 800 °C with a heating rate of 20 °C min^{-1}. Measurements were conducted with nitrogen flows of 25 and 10 cm^3 min^{-1} for the sample and balance, respectively. Films thermal stability was compared by TG curve analysis, which allows to determine the onset temperature, the decomposition temperature (measured at the peak of the differential thermogravimetric curves - DTG -), and the percentage of the residual mass. The film's moisture content was calculated from the mass loss between 25 and 200 °C.

2.8. Swelling and solubility in H₂O of films

For the determination of the swelling behaviour, four samples of each film comparable in weight were submerged in distilled water for 1, 2, 3, and 4 h at room temperature. The swelling degree was calculated by the relationship (1):

$$\text{Degree of swelling } (\%) = \frac{(W_a - W_b)}{W_b} \times 100 \qquad (1)$$

where W_b is the original dry weight of the sample and W_a is the weight after submersion in distilled water.

Swelled films were subsequently dried at room temperature up to a constant weight, and the weight loss percentage of each sample was calculated as indicated in Eq. (2):

$$\text{Weight loss } (\%) = \frac{(W_b - W_d)}{W_d} \times 100 \qquad (2)$$

where W_b is the first dry weight of film before submersion and W_d is the dry weight of the swelled film.

2.9. Dynamic mechanical analysis (DMA)

The dynamic mechanical measurements were conducted using a Q800 Dynamic Mechanical Analyzer (TA Instruments). In particular, the films were cut into rectangular-shaped portions (10.00 × 5.00 × 0.10 mm^3) and the tensile investigations were performed with a stress ramp of 5 MPa min^{-1} at 25.0 ± 0.5 °C. Measurements were performed in triplicate ($n = 3$); tensile strength and elongation at break values obtained from DMA are reported as average values with Standard Deviations (SD).

2.10. Moisture content and absorption of starch-based films

2.10.1. Initial moisture content

Starch films were cut in small sections (1 cm$x$1 cm) and their initial weight (W_i) was measured. Film pieces were then pre-dried in a dessicator containing dried silica gel (0 % RH) for 5 days at 25 °C and weighted (W_d) to calculate the initial moisture content (M_i, percentage dry basis) as follows:

$$M_i = \frac{(W_i - W_d)}{W_d}$$

2.10.2. Determination of the equilibrium moisture content

Starch film sections (1 cm × 1 cm) were placed in a dessicator at 25 °C containing a saturated solution of sodium chloride (NaCl) to mimic a storage setting with 75 % RH. The air moisture and temperature inside the dessicator was monitored through a digital temperature- and humidity-meter. Film sections were weighted after 2 and 5 h of treatment and each 24-h until the difference in weight between two consecutive measurements was smaller than 1 % - i.e., when the equilibrium moisture absorption (M_e) was reached [38]. The latter was determined by using the equation:

$$M_e = \frac{W_e}{W_i}(M_i + 1) - 1$$

where W_i, M_i, and W_e are the initial weight, the initial moisture content, and the equilibrium weight of the samples, respectively. Subsequently, samples were dried in an oven at 105 °C for 24-h to evaluate their moisture content (MC) [39]. These experiments were performed in triplicate ($n = 3$) per each starch-based film.

2.10.3. Moisture curve and rates

Moisture adsorption data obtained over the timeframe described in 2.10.2 were fitted according to the Peleg mathematical model [40]:

$$M_t = M_i + \frac{t}{k_1 + k_2 t}$$

where Mt is the moisture at the considered time, k_1 the Peleg rate constant, and k_2 the Peleg capacity constant. Fittings were performed using OriginPro software.

3. Results and discussion

3.1. Microscopic characterization of starch-based films

3.1.1. ATR-FTIR spectroscopy

3.1.1.1. Cross-linker effect and its interaction with starch. ATR-FTIR spectra of the S film, the cross-linkers CA and SC, and S_CA and S_SC binary films are shown in Fig. 1. The starch film features characteristic signals at 3316 (O—H stretching), 1150 and 1078 cm^{-1} (C—O—H stretching), and 1012 and 993 cm^{-1} (C—O—C stretching) [41].

The spectrum of CA shows typical bands at 1754, 1720, and 1683 cm^{-1} attributed to the stretching vibrations of carboxyl groups [42].

The spectrum of the S_CA film resembles that of the S film. Yet, we noticed the appearance of a broad peak at 1715 cm^{-1} (Fig. 1c), which refers to the C=O stretching vibrations. This signal can derive from a possible combination of vibration of esters bonds and free carboxyl C=O groups in CA units, being unlikely that all the starch carboxyls are
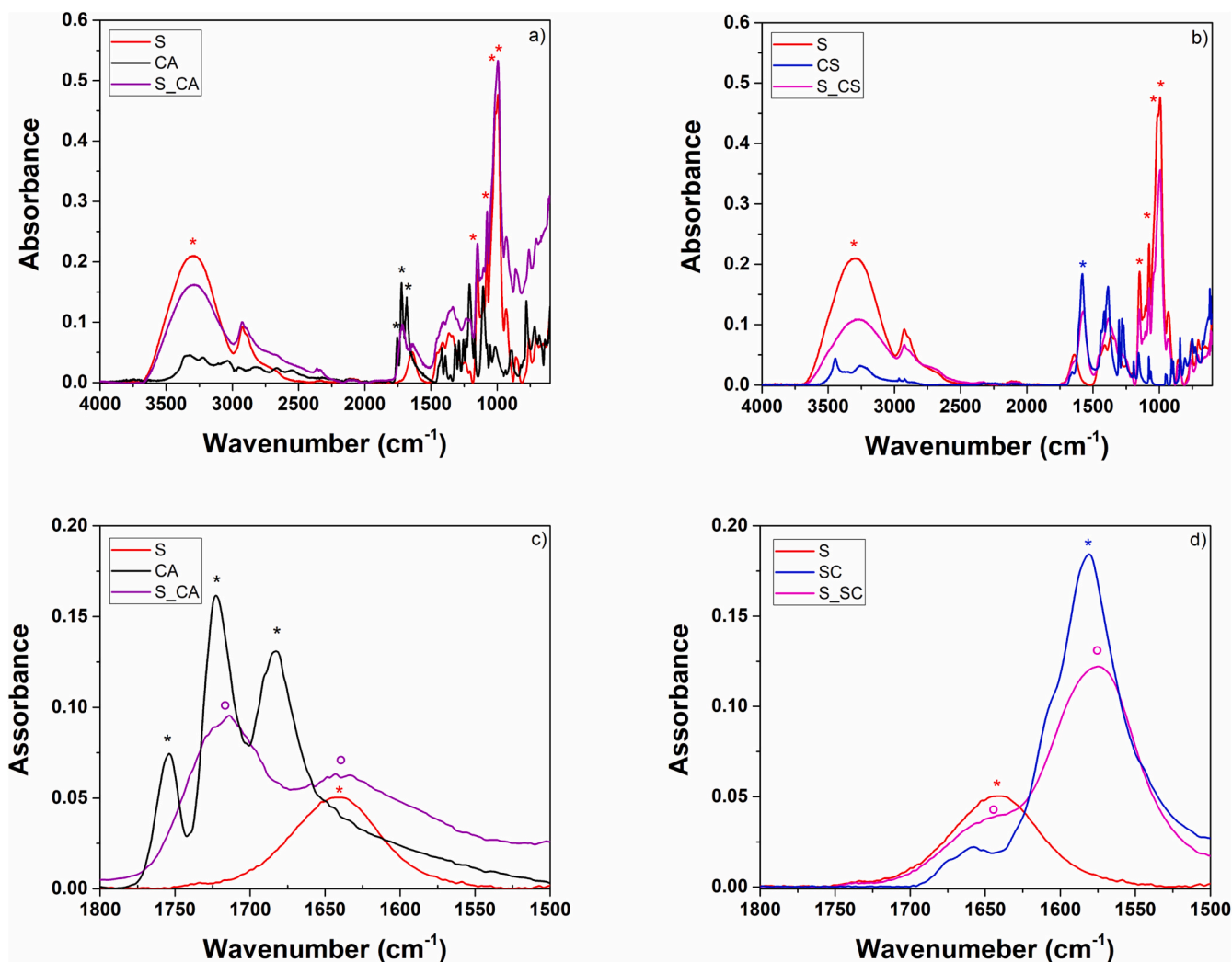
Fig. 1. ATR-FTIR spectra of a) S, CA and S_CA films, b) S, SC and S_SC films and c, d) relative magnification of the spectral region from 1800 to 1500 cm^{-1}. Symbols (*), (*) and (*) identify the characteristic peaks of S, CA, and SC. Symbols (°) and (°) identify the characteristic peaks of S_CA and S_SC.

esterified [26]. This hypothesis was confirmed by the deconvolution of the ATR-FTIR spectrum, which shows two peaks at 1710 cm^{-1} and 1735
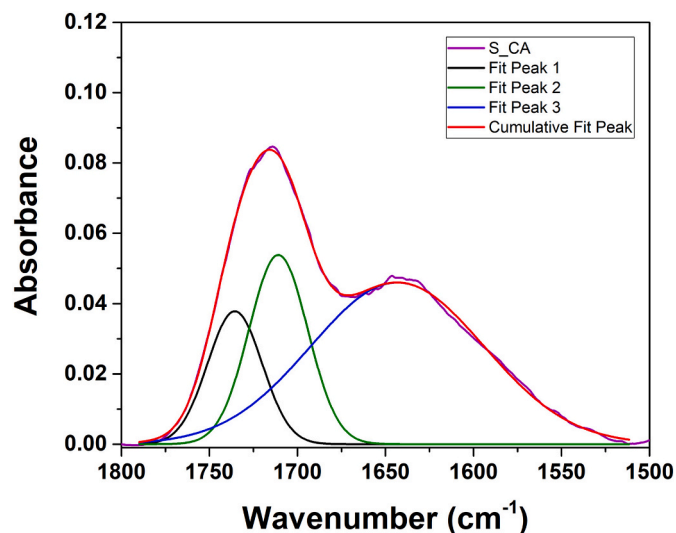

Fig. 2. ATR-FTIR spectral deconvolution by non-linear least-squares fitting of S_CA spectrum in the spectral region from 1800 to 1500 cm^{-1}.

cm^{-1} (Fig. 2). The latter is typical of the ester bonds, which can derive from the reaction between the —COOH in CA and —OH in starch [42,43]. The —OH contribution (3300 cm^{-1}) is less intense in the S_CA film than in the S film, indicating that the OH groups of starch were consumed by citric acid to generate ester linkages [26,42,44]. Finally, the band at 1640 cm^{-1} observed in the S_CA film is attributable to the —OH bending contribution of starch-bound water. The spectral evidence demonstrates chemical cross-linking with covalent bond formation between CA and starch [45,46].

The SC spectrum shows a characteristic band typical of the asymmetric —COO$^-$ (ca. 1580 cm^{-1}) stretching vibrations (Fig. 1b and d). The latter was also present in the ATR-FTIR spectrum of the S_SC film, while the -C=O stretching contributions partially overlapped with the IR absorbance deriving from the —OH bending of water in the S film (Fig. 1b and d). Moreover, the S_CS film featured a lower absorbance at 1640 cm^{-1} than the S film, and no left shoulder of the band at 1540 cm^{-1} was detected (Fig. 1b and d). These outcomes indicate the occurrence of non-covalent interactions between the citrate salt and the starch, which suggest that SC only plays the role of physical plasticizer under the preparation conditions explored.

3.1.1.2. Effect of plasticizer and interaction with starch. PEG200 was added as a plasticizer to S_SC (fixed SC/PEG200 ratio at 4) and S_CA (different amounts, Section 2.2) dispersions to optimize the properties of

these films. ATR-FTIR spectra of S_SC and S_SC_PEG200 films are shown in Fig. 3. The -OH stretching vibration peak at about 3274 cm^{-1} of the plasticized binary starch film with PEG200 is more intense than that of S_SC film and, for both, shifts to lower wavenumber respect to pure starch film (3295 cm^{-1}; Fig. 1b). This reflects that plasticizer can destroy the interaction between starch molecules to some extent and combine with starch by hydrogen bonding, as reported by Zhang and colleagues [16].

ATR-FTIR spectra of S_CA_PEG200 ternary films obtained using various CA/PEG200 ratios showed the highest differences in the 4000–2500 cm^{-1} and 1200–900 cm^{-1} spectral regions (Fig. 4). Ternary films display a higher IR absorbance associated with the O—H stretching vibration peak (ca. 3300 cm^{-1}) than binary film. Moreover, this contribution shifts to greater wavenumbers as the PEG200 amount increases. Films featuring elevated PEG200 content also show a shift of the starch —C—O vibration peak from approximately 995 cm^{-1} to 999 cm^{-1}. The latter indicates that large PEG200 quantities could partially impair starch structure and favour its interaction with water molecules, as this peak is sensitive to water content [41]. Specifically, a high amount of bound water promotes starch retrogradation [47], which determines extensive interchain H-bonding in amylopectin and amylose molecules [48–50]. The evidence gathered through ATR-FTIR spectroscopy suggests that a small amount of PEG200 in the S_CA binary film inhibits starch crystallization events. Indeed, when the amount of CA is higher or equal to PEG200, the —C—O IR absorbance does not significantly change (Fig. 3b), thus indicating a competing effect of CA and PEG200.

3.1.1.3. Starch retrogradation. Retrogradation consists of the formation of crystalline structures, which cause detrimental effects in foods and materials containing starch [51]. Nevertheless, additives (e.g., proteins, salts, acids, polyols, and other polysaccharides) can partially prevent this phenomenon [40].

Several physical-chemical techniques can assist in evaluating the starch crystal structure, among which FTIR spectroscopy plays a crucial role [52]. In particular, the latter allows obtaining information on the degree of starch short-range order by monitoring the bands in the 1200–900 cm^{-1} region, which is sensitive to changes in polysaccharide structure [51]. Indeed, according to Kim et al. [19], starch retrogradation determined the splitting of the —C—O (in C—O—C) asymmetric stretching vibration signal at 1018 cm^{-1} into three peaks at 1050 cm^{-1}, 1018 cm^{-1}, and 995 cm^{-1}. The band at 1050 cm^{-1} relates to the ordered

phase of starch [53], whereas contributions at 1018 cm^{-1} and 995 cm^{-1} represent the amorphous one. The 995-to-1018 cm^{-1} ($A_{995/1018}$) and the 1050-to-1018 cm^{-1} ($A_{1050/1018}$) band area ratios indicate the ability to inhibit starch retrogradation [48] and the degree of order in starch polymers, identifying the crystalline structure region in the amorphous area [18], respectively. Thus, these ratios (Table 2) were calculated on peak areas obtained by performing deconvolutions of ATR-FTIR spectra of the prepared starch-based films in the 1200–900 cm^{-1} region (Figs. S1–S2).

The smaller the $A_{995/1018}$ ratio, the stronger the starch retrogradation is inhibited. Taking the value of the $A_{995/1018}$ ratio for starch as a reference, the sole PEG200 does not alter the retrogradation process (Table 2). The S_CS and S_CS_PEG200 films have lower ratios than the S film, indicating that SC and, better still, its combination with PEG200 inhibits starch retrogradation. For ternary S_CA_PEG200 films, retrogradation depends on the amount of PEG200. Indeed, a high amount of PEG200 favours retrogradation. The retrogradation process is inhibited when the CA/PEG ratio is 4. The amount of PEG200 also influenced the crystalline structure of the S_CA_PEG200 ternary films (Table 2). Indeed, increasing PEG200 amounts favour starch recrystallization, as highlighted by the high $A_{1050/A1018}$ ratios (Table 2), while the sole addition of CA (S_CA) caused no apparent variations in the degree of crystalline order. Based on these results, a small amount of PEG200 can efficiently improve the compatibility between starch and CA [21], making the ternary film more stable and inhibiting the polysaccharide retrogradation and recrystallization [19].

3.1.1.4. Aging effect. The aging of starch and plasticized starch films were studied by performing ATR-FTIR spectroscopy on one-year-old S, S_PEG200, S_SC, S_CA, S_SC_PEG200, and S_CA_PEG200 films. The obtained spectra showed comparable vibrational modes (i.e., peak presence and position) than newly produced films (Fig. 1; Fig. S3), indicating the maintenance of their structure in time. The long-term retrogradation deriving from recrystallisation of amylopectin [54] was determined by calculating the $A_{995/1018}$ and $A_{1050/1018}$ ratios (Table 3) from spectral deconvolutions in the 1180–880 cm-1 region (Fig. S4).

The calculated ratios did not significantly change after one year of film storage, and ternary films were more stable over time than binary ones (Table 3). These results demonstrate once again that co-plasticizers in appropriate proportions more effectively hinder starch retrogradation than the single plasticizer and suggest the suitability of these starch-based films for applicative purposes even after one year from their preparation.

3.1.2. ss-NMR spectroscopy

The structure of starch-containing films and the structural changes of this polysaccharide induced by SC, CA, and PEG200 were investigated through ^{13}C[^{1}H] CP-MAS solid-state NMR spectroscopy (Fig. 5). All films feature signals in the regions 90–110, 80–90, 67–80 and 58–67 ppm, which correspond to C1, C4, C2,3,5 and C-6 carbon of starch [55].

The S_CA_PEG200 ternary film (red spectrum) presents some peculiarities. The signal of C6 carbon appears as the superimpositions of at least three components centred at 64.1, 62.1, and 59.5 ppm, which suggests significant changes in the orientation of the O6 group [56]. In addition, the shoulder at ca. 75 ppm of the band relating to the signals of C2,3 and 5 is shifted at a lower chemical shift value. According to the literature [57], the not-resolved peaks in the 80–67 ppm region can also derive from C2, C3, and C5 with substitution groups, such as the ester groups in modified starch. This shift could indicate that the carboxyl group of citric acid cross-links with the carbon 2 and 6 of starch. The presence of this shoulder in S_SC, S_PEG200, and S_SC_PEG200 films may relate to hydrogen bonds between starch and SC or PEG200 that can modify the chemical neighbour of C2 and C3. In all ^{13}C CPMAS spectra, the chemical shift and peak shape of the C1 signal differed (Fig. 5), giving information on starch polymorphisms, as this peak is more
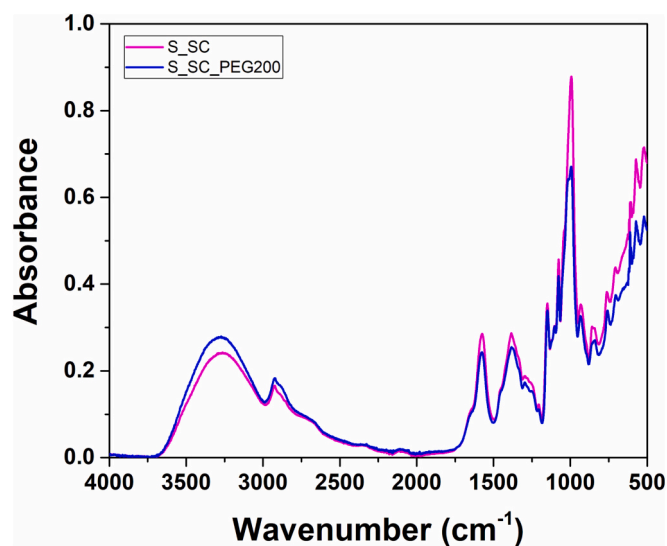

Fig. 3. ATR-FTIR spectra of S_SC binary film and S_SC_PEG ternary film with SC/PEG200 weight ratio of 4:1.
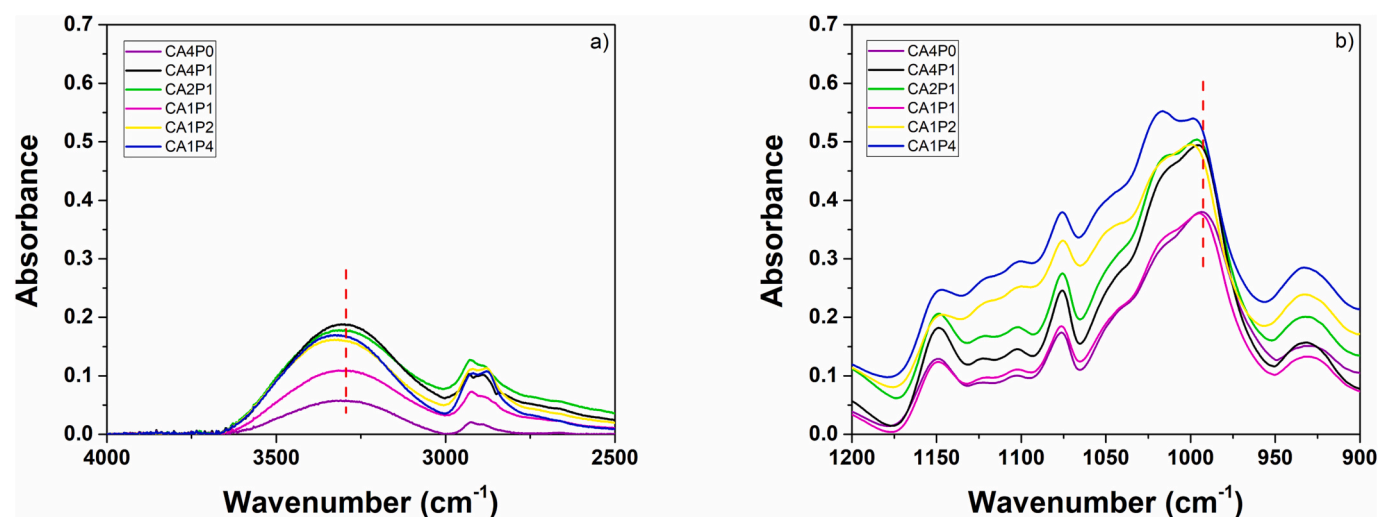
Fig. 4. ATR-FTIR spectra of S_CA_PEG200 films at different CA/PEG200 weight ratios. Spectral region a) 4000 to 2500 cm^{-1} b) 1200 to 900 cm^{-1}.

Table 2
Values of peak area ratios at 995 and 1018 cm^{-1} (A$_{995/1018}$) and 1050 and 1018 cm^{-1} (A$_{1050/1018}$).

Sample	A$_{995/1018}$	A$_{1050/1018}$
S	6.6 ± 0.8	3.5 ± 0.5
S_PEG200	5.9 ± 0.7	3.6 ± 0.5
S_SC	4.6 ± 0.5	2.9 ± 0.4
S_SC_PEG200	4.1 ± 0.5	2.7 ± 0.4
S_CA	7.6 ± 0.9	3.3 ± 0.4
S_CA/PEG200 (4)	5.3 ± 0.7	2.8 ± 0.4
S_CA/PEG200 (2)	6.7 ± 0.7	3.1 ± 0.4
S_CA/PEG200 (1)	7.8 ± 1.4	4.8 ± 0.8
S_CA/PEG200 (0.5)	8.4 ± 1.3	5.4 ± 1.3
S_CA/PEG200 (0.25)	8.4 ± 1.4	5.5 ± 1.3

Table 3
Values of peak area ratios at 995 and 1018 cm^{-1} (A$_{995/1018}$) and 1050 and 1018 cm^{-1} (A$_{1050/1018}$) for aged starch films.

Sample	A$_{995/1018}$	A$_{1050/1018}$
a-S	10 ± 3	5.0 ± 1.0
a-S_PEG200	3.9 ± 0.7	3.2 ± 0.8
a-S_SC	4.8 ± 0.7	3.3 ± 0.6
a-S_SC_PEG200	3.5 ± 0.5	2.8 ± 0.4
a-S_CA	5.3 ± 0.8	2.5 ± 0.4
a-S_CA/PEG200 (4)	4.0 ± 0.4	1.5 ± 0.2

a indicates aged films.

sensitive to starch conformational changes than C2, C3, and C5. Indeed, the C1 signal shows higher chemical shift dispersion under the variation of the torsion angles of the glycosidic linkage in α-(1,4) glucans than the other starch carbons [58]. In amorphous starch, the broad distribution of conformations thus leads to a large chemical shift dispersion of the C1 peak. The C1 splitting of the crystalline forms results from the different space groups adopted by A and B forms, which display three or two peaks at 100.4, 99.2, and 98.2 ppm or 100.0 and 99.2 ppm, respectively [58]. The starch-based films in this study showed a characteristic envelope of signals in the 93.0–106.0 ppm region with a maximum between 103.0 and 104.0 ppm, typical of amorphous materials. Specifically, the amorphous content is the highest in the S_SC_PEG200 and S_CA_PEG200 ternary films. The S_CA and S_SC binary films also showed an up-field shoulder at about 100.4 ppm, typical of double helical conformations, which was more defined and intense in the latter (Fig. 5). This increased double helix content may partly be derived from the increase in linear chains derived from retrograded partially

hydrolysed amylose or branched portions of amylopectin [55]. According to the literature [59], an amylose-rich starch has a more amorphous/mobile structure; thus, amylose can also undergo recrystallization processes [60], consistent with the high flexibility of amylose.

Comparing S_SC, S_CA, S_SC, PEG200, and S_CA_PEG200 NMR spectra reveals that PEG200 is crucial to improve the ternary film quality as, for instance, PEG200 presence prevents the recrystallization of starch. Moreover, these results agree with our previous observations obtained through ATR-FTIR spectroscopy.

3.1.2.1. Relaxation kinetics. NMR relaxometry techniques were used to assess the dynamics of molecular motions in starch-based films. To detect dynamic changes in the polymer induced by SC or CA and PEG200, the carbon spin-lattice relaxation times in the rotating frame, T$_{1\rho}$(C), were determined as described in Section 2.5 and reported in Table 4.

Since T$_{1\rho}$(C) gives information about molecular motions in the kHz range [61], it accounts for the polymeric chain's dynamic behaviour in a few nanometers range, being a suitable probe for local mobility. The S film denotes the slowest relaxation rate, which indicates its stiffness, while the three binary systems reveal similar behaviours. The ternary systems feature the lowest T$_{1\rho}$(C) values, yet the S_SC_PEG200 film displays a significantly lower value than the S_CA_PEG200 one.

T$_{1\rho}$(C) values are complemented by evaluating the NMRD and relevant IIT curves derived from FFC data (Fig. 6a and b), whose values reflect molecular motions differently from T$_{1\rho}$(C). Indeed, slower molecular motions are accounted for by slower relaxation and larger T$_{1\rho}$(C) values.

The brittle S film shows no fast dynamics, as Monte Carlo analysis affords only an apparent maximum (cut off in Fig. 6b) at 4 ± 1 μs, whereas S_CA features only a dynamic component at 0.19 ± 0.03 μs. The latter accounts for the much larger molecular mobility of starch chains for S_CA than S film, which indicates a higher microscopic disorder. This phenomenon derives from the modifications determined by the partial esterification of the glucose subunits of starch from CA, which likely hampers, at least partially, intra-chain hydrogen bonding. In the case of the S_PEG200 film, the IIT curve features both a short-time dynamic component at 0.11 ± 0.01 μs and a slow one at 6 ± 1 μs, suggesting a more disordered and mobile situation than for the S film. Nevertheless, the hydrogen bonding disruption deriving from PEG is less effective than in the previous case. On the opposite, the IIT curve of the S_SC film features a wide distribution at 1.0 ± 0.3 μs, indicating that SC can modify the hydrogen bonding network of starch. Yet, the SC effect cannot be compared with CA or PEG200, as significant stiffness still
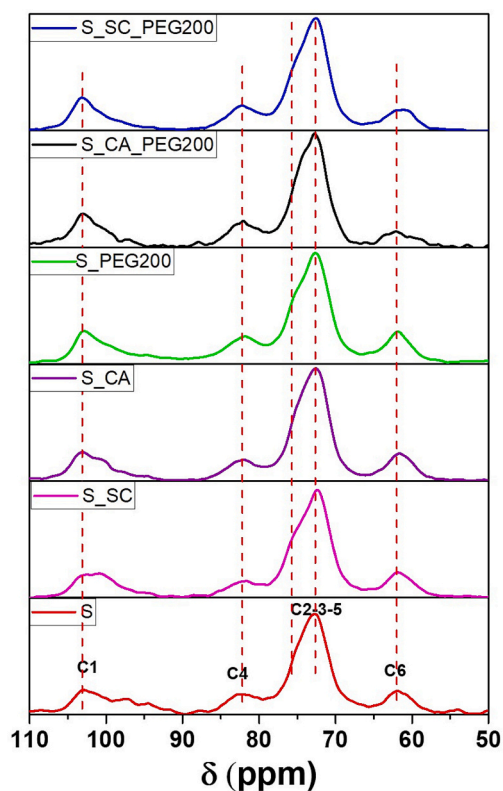
Fig. 5. $^{13}C[^{1}H]$ CP-MAS solid-state NMR spectra of the S film; S_PEG200, S_CA, S_SC binary films, and S_CA_PEG200 (20 wt% CA vs. starch mass and AC/PEG200 = 4) and S_SC_PEG200 (20 wt% SC vs. starch mass and SC/PEG200 = 4) ternary films.

Table 4
$T_{1\rho}(C)$ values for the C2-3-5 contribution in the ^{13}C NMR spectrum of starch films, binary and ternary films.

Sample	$T_{1\rho}C$ (ms)
S	17 ± 2
S_PEG200	9 ± 1
S_SC	10 ± 2
S_ SC_PEG200	4.0 ± 0.5
S_CA	10 ± 1
S_CA_PEG200	7.4 ± 0.9

occurs in the material.

On passing to ternary systems, the S_CA_PEG200 film shows an IIT profile similar in shape to the S_PEG200, even though a significant downshift of the apparent correlation times was observed in the former, as the fast component is at 44 ± 7 ns and the slow one at 1.3 ± 0.3 μs. Hence, the intra-chain hydrogen bonding network of starch is efficiently disrupted by the simultaneous presence of the cross-linker CA and the plasticizer PEG200, which also determines the best mobility at a microscopic level. Finally, the IIT curve for the sample S_SC_PEG200 displays a broad distribution in the slow-motion region (with an apparent maximum at 1.1 ± 0.4 μs) and a broad fast component at 80 ± 30 ns, roughly comparable with the other ternary film. This outcome
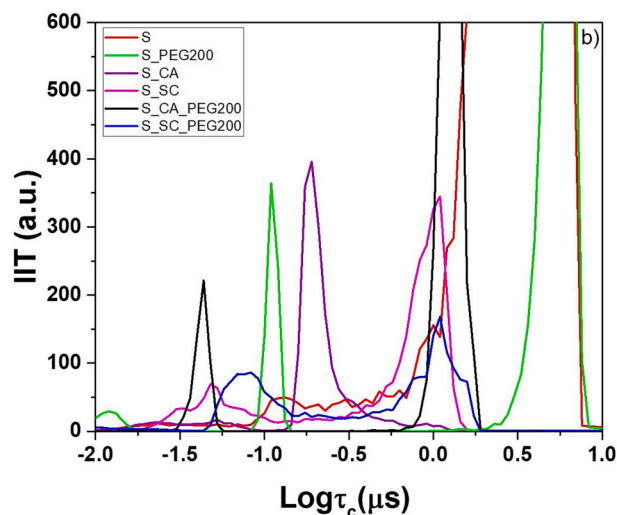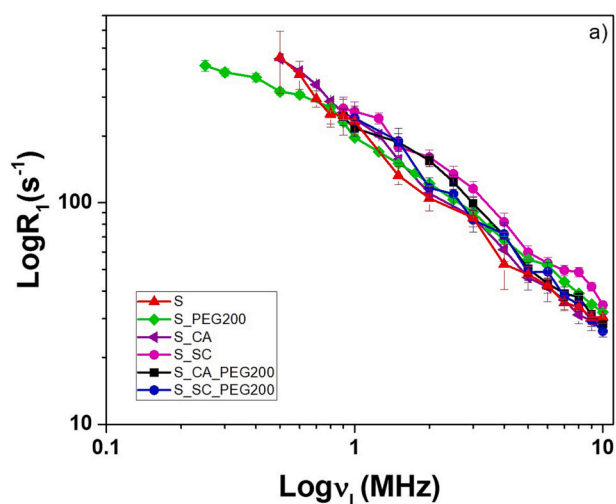

Fig. 6. a) NMRD curves and b) IIT curves of the starch-based films.

confirms, on one side, the beneficial effect of combining a cross-linker with a plasticizer and, on the other, the less efficient cross-linker action of SC than its acidic counterpart CA.

Differences between these results and those obtained through $T_{1\rho}(C)$ evaluation trace back to the diverse aspect of systems dynamics that the latter focuses on, namely the intrinsic mobility of the glucose subunit backbone. Overall, relaxometry data indicate that SC has a more significant effect than CA or PEG200. This diversity likely derives from the strong hydrogen bonding between the anionic salt units and the glucose subunits, which can facilitate their torsional motion but exert less disordering effect on the arrangement of starch chains.

3.1.3. Crystalline structure of starch-based films using XRD analysis

The crystal structure of starch-based films, alongside their degree of crystallinity (DC; the percentage of crystalline regions to the total material), are significant to consider, as they influence films' physical, mechanical, and technological properties.

XRD patterns of starch films are shown in Fig. 7. Spectrum of S film presented low intensity, broad diffraction peaks, and a high amorphous scattering halo, features typical of a semicrystalline polymer with low crystallinity [29]. Diffraction peaks at 5.6°, 17°, 19.6°, 22.1° and 23.8° in the starch film are the characteristic peaks of B-type crystal [12,29]. Starch-based binary and ternary films show some of these signals, yet XRD patterns reveal significant modifications than the S film. This evidence aligns with the measured DCs (Table 5).

Binary S-CA film features a DC comparable to the S film, while a higher value was measured for S_PEG200 and S_CA. The latter phenomenon may derive from a hydrolysis effect exerted by the plasticizer or the cross-linker [29], which can slightly promote starch crystallization under the conditions used for film' preparation. In contrast, S_SC and S_SP_PEG200 films displayed small DCs, being the lowest for the ternary one. This outcome reiterates the efficiency of the SC-PEG200 co-plasticizing effect in hindering starch recrystallization during film formation and decreasing the crystalline starch portion, preventing its retrogradation.

3.2. Macroscopic properties of starch-based films

3.2.1. Thermal stability

High thermal stability is one of the functional applicative features of new materials with low environmental impact [62] and great interest in industrial applications [63,64]. Thermograms provide crucial
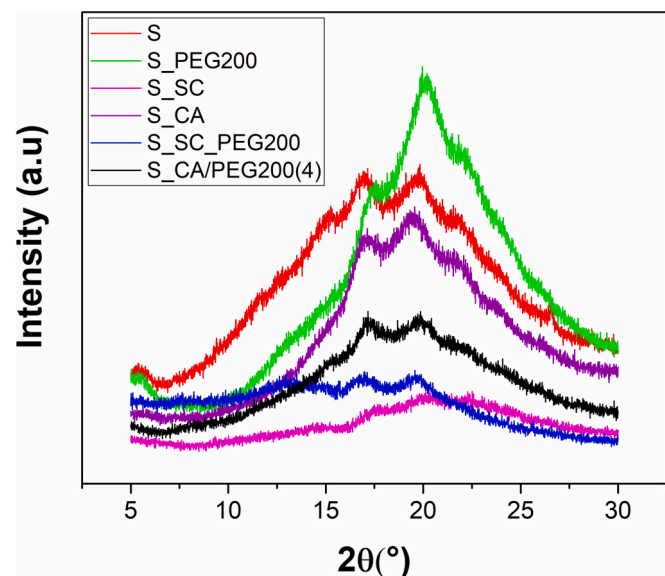

Fig. 7. XRD patterns of starch-based films.

Table 5
Degree of crystallinity (DC) of starch-based films.

Sample	DC
S	26.4
S_PEG200	31.3
S_SC	17.8
S_ SC_PEG200	14.1
S_CA	28.9
S_CA_PEG200	25.4

information regarding polymeric materials' thermal stability and degradation [65]. The initial weight loss observed for all starch-containing films in the 25–200 °C range was attributed to the loss of physisorbed water [46], which was the highest for the S film (Fig. 8).

PEG200 does not substantially influence the starch thermal behaviour, as highlighted by the similarities between S and S_PEG200 thermograms (Fig. 8). In contrast, the cross-linker addition triggered starch degradation at a lower temperature than S or S_PEG200 films (Fig. 8). Both cross-linkers slowed the film degradation process in the 300–550 °C range. Yet, SC more efficiently stabilized the S_SC, as a 5 % residual mass was obtained at temperatures above 600 °C, whereas the S_CA completely degraded at 550 °C (Fig. 8). These results suggest that the intermolecular non-covalent interactions between SC and starch led to change at a microscopic level that reflects, at the macroscopic level, on the film's thermal stability. The degradation of ternary films appears more complex, likely due to the simultaneous presence of cross-linker and PEG200, which may synergistically protect the starch polymer. The degradation process of S_CA_PEG200 and S_SC_PEG200 films is completed at ca. 730–770 °C, yet the latter featured a 7 % residual mass at 800 °C (Fig. 8a). Moreover, adding SC to the ternary films led to a more gradual mass loss up to about 320 °C, and a decreased degradation rate decreases in the 320–640 °C range than CA (Fig. 8). The higher thermal stability conferred to ternary films by SC than CA may derive from the extension and stabilisation of the hydrogen bonds network involving starch and PEG200.

3.2.2. Degree of swelling and water solubility of ternary films

The degree of swelling (DS) and water solubility of polysaccharide-based films are fundamental parameters for their application in food packaging or biomedicine, to name a few. For instance, the DS can help determine the cross-linking degree, the degradation rate, and the mechanical or viscoelastic properties of polysaccharide hydrogels or films [66]. The DS calculated for starch-containing ternary films over a 4-h submersion timeframe is shown in Fig. 9a. Overall, the S_SC_PEG200 film displayed a lower DS than the S_CA_PEG200 film, indicating that the former absorbs less water and is more stable in this solvent. Specifically, the DS of the S_CA_PEG200 film increased abruptly as a function of the submersion time, reaching a value of 300 % after 4-h submersion (Fig. 9a).

The water solubility resistance of polysaccharide-based films becomes important when their application involves their contact with water for the desired timeframe [67]. The water solubility of hydrogels or films is generally expressed as their weight loss percentage after submersion. In general, cross-linked starch macromolecules cause an increase in the resistance of films to disarm, allowing their swelling [43], as in this case of starch films amended with CA (Fig. 9a and b). Therefore, in agreement with the ATR-FTIR results, citric acid effectively cross-links starch, prevents its dissolution, and considerably decreases the weight loss of the films in water. Comparing the ternary films, the lower weight loss of the S_CS_PEG200 film than the CA_S_PEG200 film (Fig. 9b) indicates the lower solubility of the former [68]. This evidence, alongside the swelling behaviour, reveals a higher water resistance for the S_SC_PEG200 film, which, by acting as a physical barrier, inhibits water absorption, the first step of biodegradation [69]. Based on the results obtained, SC in starch films prevents the swelling of starch
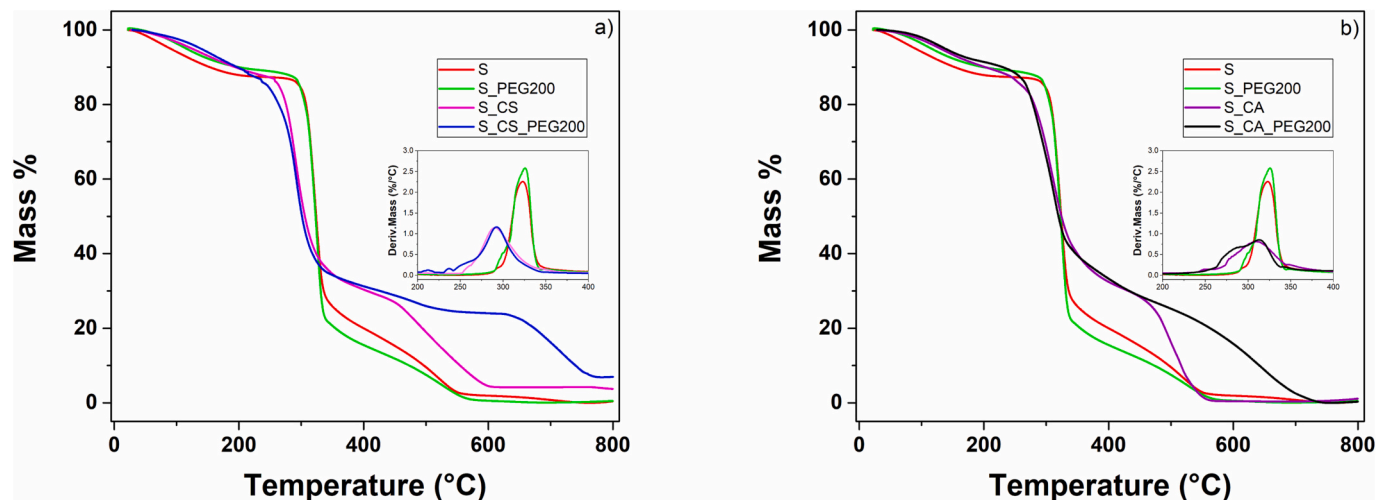
Fig. 8. TGA curves of a) S, S_SC, S_PEG200, and S_SC_PEG200 (20 wt% SC compared to starch and SC/PEG = 4) films, and b) S, S_CA, S_PEG200, and S_CA_PEG200 (20 wt% CA compared to starch and CA/PEG = 4) films.
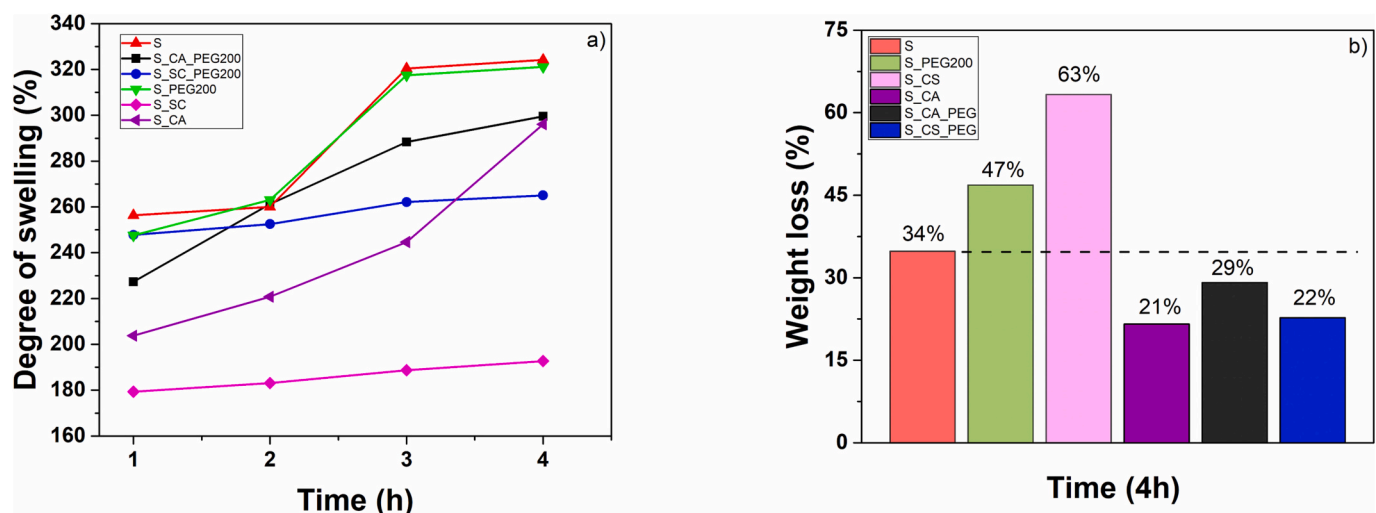

Fig. 9. a) Degree of swelling and b) weight loss (%) of starch-based films.

(Fig. 9a), while PEG200 creates a denser structure which decreases the accessible regions to water, leading to an improvement in the resistance to dissolution, compared to both S and binary S_SC films (Fig. 9b). The higher water solubility resistance and lower DS of the starch molecules are likely the main reasons for the better stability of the S_SC_PEG200 ternary film in water compared to all film systems studied. Besides, these results suggest the potential suitability of ternary starch-based films for edible food coating and encapsulation, which can require a certain degree of film solubilization [8].

3.2.3. Mechanical properties

The stress-strain experiments are one of the most used tests to characterize the mechanical behaviour of materials. In this study, the stress-strain curve obtained for the pure starch is distinctive of brittle materials, while S_CA_PEG200 and S_SC_PEG200 ternary films showed the typical behaviour of ductile materials (Fig. 10; Table 6).

Indeed, ternary films exhibited two hallmark regions of deformation behaviour in their stress-strain curves. At low strain (lower than 5 %), both the former and the stress increased rapidly. At higher strains (higher than 5 %), the films showed a slow increase in stress with strain until failure occurred. Thus, as stress-strain tests indicate the strength of a material, cross-linking and plasticizing agents' presence increases the

flexibility of the polymer chains. As a result, the elongation at break for ternary films increases, and the latter acquire a higher ductility at the expense of stiffness [70]. It is important to remark that the ternary films show discernible maximums of rupture. According to the results reported in Table 4, the S_CA_PEG200 ternary film had the greatest elongation and tensile strength. The lower mechanical strength of the S_SC_PEG200 ternary film is probably due to the dense network of hydrogen bonds, which hinders the sliding between the molecular chains and makes them less deformable.

3.2.4. Moisture content and absorption of starch-based films

The water sorption properties of the starch-based films are worth investigating to elucidate their potential application in food packaging. According to the literature, moisture sorption significantly influences the stability of starch films during packaging and storage conditions [71]. Starch is a hygroscopic material, and adding hydrophilic plasticizers, such as PEG200, may enhance the moisture absorption of starch, accelerating, in turn, its recrystallization. In this regard, water-sensitive plasticizers do not favour the application of thermoplastic starch, especially for packaging materials [16]. Therefore, the ideal plasticizer should reduce the moisture absorption of starch.

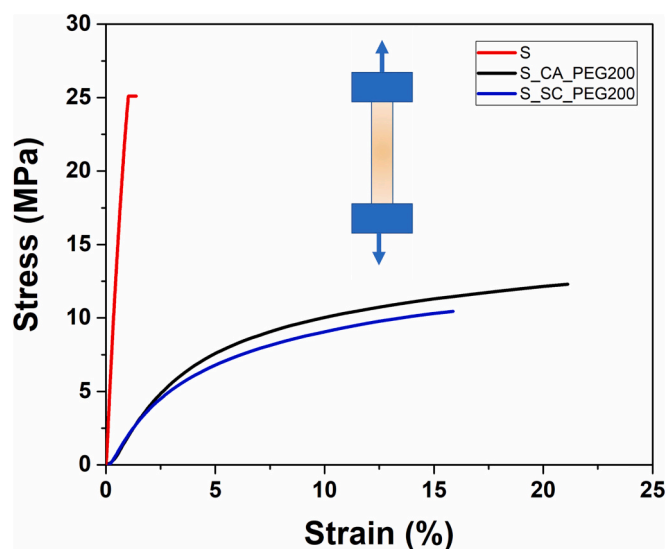Here, the moisture sorption test was performed at 25 °C and relative

Fig. 10. Stress-strain curves of S, S_CA_PEG200, and S_SC_PEG200 films. The inset displays a sketch image of the deformation.

Fig. 11. Equilibrium moisture content (M_e) of starch-based films overtime.

Table 6
Results of the parameters obtained from the tensile tests.

Sample	Tensile strength (MPa)	Elongation at break (%)
S	25.0 ± 1.0	1.40 ± 0.06
S_ SC_PEG200	10.9 ± 0.4	16.2 ± 0.7
S_CA_PEG200	12.6 ± 0.5	22.7 ± 0.9

humidity (RH) of 0 % and 75 %; the films' initial (M_i) and final (MC) moisture contents are reported in Table 7.

The MC values of binary and ternary starch-based films are lower than those of S film (Table 5). In agreement with previous results [16,72], the strong hydrophilicity, the high number of water-binding sites, and the weak ability of PEG200 to associate with starch promote films' moisture adsorption. Indeed, S_PEG200 features a higher M_i than the starch film, while the MC at 75 % RH was comparable between the two samples (Table 5). Adding SC or CA to the starch polymer causes a decreased moisture sorption in the resulting films. Yet, the lowest MC value is obtained for the ternary S_SC_PEG200 film (Table 5), which likely traces back to the few water binding sites deriving from the simultaneous presence of SC and PEG200 and the subsequent changes in the starch microstructure [16]. Thus, the co-plasticizing effect of SC and PEG200 in the right proportions decreases the hygroscopic sensitivity of starch [22] by reducing moisture absorption and the moisture humidity sensitivity of the ternary film.

The kinetics of the water sorption process by starch-based films was obtained by evaluating the equilibrium moisture content (M_e) as a function of their time of storage at 75 % RH (Fig. 11). Overall, a low moisture amount is adsorbed over time by films, which achieved the equilibrium rapidly. At the initial stage (2 and 5-h), the high partial pressure of saturated vapor causes an increase in M_e for all films (Fig. 11), indicating their water sorption activity [73]. From 5-h
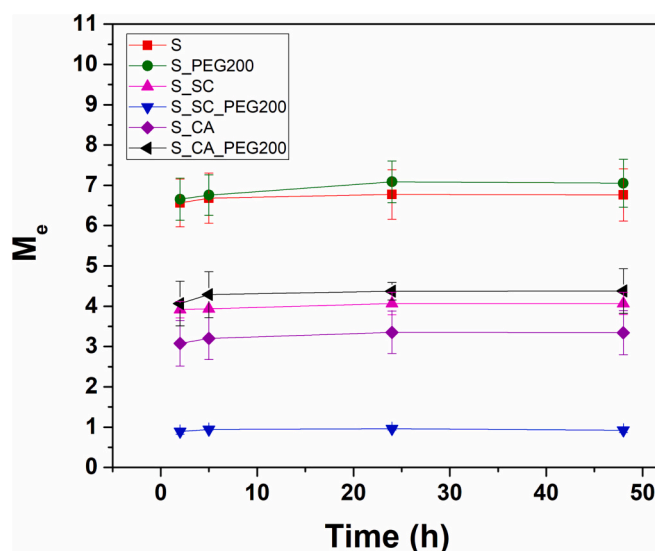
onwards, M_e reaches a plateau (Fig. 11), likely due to the elevated pressure difference between films and the surrounding water. This evidence, in turn, suggests that films became equilibrated with the RH of the storage environment [38]. Among the analysed samples, only the S_PEG200 film features an M_e kinetics higher than the S one (Fig. 11), confirming the superior ability of the former to absorb moisture from the surrounding atmosphere. In line with MC estimation, binary and ternary films show lower M_e values than S over the timeframe considered; once again, the lowest Me values are observed for the ternary S_SC_PEG200 film (Fig. 11).

A deeper investigation of the water sorption process was performed by fitting the moisture content data at the chosen times using the Peleg model [38], which allows for determining the parameters k_1 and k_2 (Table 8) related to the initial water adsorption rate and the maximum water adsorption capacity.

The S and S_PEG200 films display the lowest k_1 and k_2 values (Table 8), corresponding to the highest water adsorption rate and capacity, hence their fast and abundant water sorption during storage [38]. This phenomenon is limited in binary and ternary films, which exhibit higher Peleg constants than the starch one (Table 8). Nevertheless, the increased water-binding sites of the ternary S_CA_PEG200 film deriving from the plasticizer's presence determine higher water sorption than its binary S_CA counterpart (Table 8). On the opposite, the co-plasticizing effect of SC and PEG200 results in the highest k_1 and k_2 values (Table 8), which further confirms the limited ability of the S_SC_PEG200 film to absorb water from the environment. Overall, analysing the moisture content and adsorption corroborate the swelling and water solubility tests, *ss*-NMR and ATR-FTIR spectroscopy findings, even one year after the film's preparation.

Table 7
Initial (M_i) and final (MC) moisture content of starch-based films.

Sample	M_i (0 % RH)	MC
S	6.6 ± 0.7	5.8 ± 0.6
S_PEG200	6.8 ± 1.4	5.4 ± 1.0
S_SC	3.9 ± 1.7	2.8 ± 0.9
S_ SC_PEG200	0.6 ± 0.1	0.8 ± 0.01
S_CA	3.1 ± 1.0	2.9 ± 0.9
S_CA_PEG200	4.2 ± 0.6	3.9 ± 0.5

Table 8
Constant values and correlation coefficient for water sorption curves fitted with Peleg model of starch-based films at 75 % RH.

Sample	k_1	k_2	R^2
S	0.16 ± 0.05	0.19 ± 0.02	0.998
S_PEG200	0.44 ± 0.08	0.38 ± 0.03	0.987
S_SC	3.1 ± 0.2	0.68 ± 0.1	0.989
S_SC_PEG200	18 ± 2	4.2 ± 0.4	0.998
S_CA	3.4 ± 0.7	2.1 ± 0.4	0.985
S_CA_PEG200	1.6 ± 0.6	0.80 ± 0.02	0.998

4. Conclusions

In this study, some micro and macroscopic properties of starch (S) -based films, obtained through solvent-casting aqueous starch dispersions containing cross-linkers and plasticizers agents, were explored. Citric Acid (CA) or sodium citrate (SC) and polyethylene glycol (PEG200) were used as cross-linkers and a plasticizer, respectively, alone or combined in different weight ratios. CA binds effectively to S through the formation of covalent bonds, while SC plays the role of a physical plasticizer. In both cases, adding small quantities of PEG200 efficiently improves the stability of S film by inhibiting the retrogradation and recrystallization processes and increasing the mobility of polymer chains. This effect was observed the most for the S_SC_PEG200 ternary film, which was the more stable. Yet, although this ternary film features greater mobility of the polymeric chains, which implies greater flexibility at the expense of the rigidity (typical of the S film), the S_SC_PEG200 showed a lower elongation resistance at break than the S_CA_PEG200. This lower mechanical strength likely derives from the dense network of hydrogen bonds that, on the one hand, hinders sliding between the molecular chains and, on the other, acts as a kind of physical barrier, making the structure more stable to thermal degradation and inhibiting water absorption. The microscopic evidence observed can be correlated and justify the variations in the macroscopic properties of the modified starch films. Thus, these results demonstrate that investigating the microscopic behaviour of starch-based films and, more generally, a polymer matrix is crucial to predict the macroscopic properties of these materials, which, in turn, are essential to developing innovative materials.

CRediT authorship contribution statement

Veronica Ciaramitaro: Methodology, Validation, Formal analysis, Investigation, Data curation, Writing – original draft, Visualization. **Elena Piacenza:** Conceptualization, Methodology, Formal analysis, Writing – original draft, Visualization. **Paolo Lo Meo:** Conceptualization, Methodology, Formal analysis, Data curation, Writing – review & editing. **Calogero Librici:** Validation, Investigation. **Martina M. Calvino:** Validation, Formal analysis, Investigation. **Pellegrino Conte:** Conceptualization, Resources, Writing – review & editing. **Giuseppe Lazzara:** Resources, Writing – review & editing. **Delia F. Chillura Martino:** Conceptualization, Resources, Writing – review & editing, Supervision, Project administration, Funding acquisition.

Declaration of competing interest

The authors declare that they have no known competing financial interests or personal relationships that could have appeared to influence the work reported in this paper.

Appendix A. Supplementary data

Supplementary data to this article can be found online at https://doi. org/10.1016/j.ijbiomac.2023.127225.

References

[1] O. Horodytska, F.J. Valdés, A. Fullana, Plastic flexible films waste management–a state of art review, Waste Manag. 77 (2018) 413–425, https://doi.org/10.1016/j. wasman.2018.04.023.

[2] T.R. Harrison, V.K. Gupta, P. Alam, A.W. Perriman, F. Scarpa, V.K. Thakur, From trash to treasure: sourcing high-value, sustainable cellulosic materials from living bioreactor waste streams, Int. J. Biol. Macromol. 233 (2023), 123511, https://doi. org/10.1016/j.ijbiomac.2023.123511.

[3] Y. Zhou, Y. He, X. Lin, Y. Feng, M. Liu, Sustainable, high-performance, and biodegradable plastics made from chitin, ACS Appl. Mater. Interfaces 14 (2022) 46980–46993, https://doi.org/10.1021/acsami.2c12764.

[4] S. Wang, P. Zhang, Y. Li, J. Li, X. Li, J. Yang, M. Ji, F. Li, C. Zhang, Recent advances and future challenges of the starch-based bio-composites for engineering applications, Carbohydr. Polym. 307 (2023), 120627, https://doi.org/10.1016/j. carbpol.2023.120627.

[5] D. Zhu, M. Li, C. Fang, J. Yu, Z. Zhu, Y. Yu, Y. Shao, Effects of storage on the starch fine structure and physicochemical properties of different rice variety types, Carbohydr. Polym. 300 (2023), 120273, https://doi.org/10.1016/j. carbpol.2022.120273.

[6] C. Leites Luchese, P. Benelli, J.C. Spada, I.C. Tessaro, Impact of the starch source on the physicochemical properties and biodegradability of different starch-based films, J. Appl. Polym. Sci. 135 (2018) 46564, https://doi.org/10.1002/app.46564.

[7] N. Nang, W. Gao, F. Zou, H. Tao, L. Guo, B. Cui, L. Lu, Y. Fang, P. Liu, Z. Wu, The relationship between molecular structure and film-forming properties of thermoplastic starches from different botanical sources, Int. J. Biol. Macromol. 230 (2023), 123114, https://doi.org/10.1016/j.ijbiomac.2022.123114.

[8] E. Basiak, A. Lenart, F. Debeaufort, Effect of starch type on the physico-chemical properties of edible films, Int. J. Biol. Macromol. 98 (2017) 348–356, https://doi. org/10.1016/j.ijbiomac.2017.01.122.

[9] D. Domene-Lopez, J.C. Garcia-Quesada, I. Martin-Gullon, M.G. Montalban, Influence of starch composition and molecular weight on physicochemical properties of biodegradable films, Polymers 11 (2019) 1084, https://doi.org/ 10.3390/polym11071084.

[10] D. Domene-Lopez, J.J. Delgado-Marin, I. Martin-Gullon, J.C. Garcia-Quesada, M. G. Montalban, Comparative study on properties of starch films obtained from potato, corn and wheat using 1-ethyl-3-methylimidazolium acetate as plasticizer, Int. J. Biol. Macromol. 135 (2019) 845–854, https://doi.org/10.1016/j. ijbiomac.2019.06.004.

[11] J.R. Vaz Matheus, R.R. Dalsasso, E.A. Rebelatto, K.S. Andrade, L.M. de Andrade, C. J. de Andrade, A. Rodrigues Monteiro, A.E. Cavalcante Fai, Biopolymers as green-based food packaging materials: a focus on modified and unmodified starch-based films, Compr. Rev. Food Sci. Food Saf. 22 (2023) 1148–1183, https://doi.org/ 10.1111/1541-4337.13107.

[12] A. Lopez-Rubio, B.M. Flanagan, E.P. Gilbert, M.J. Gidley, A novel approach for calculating starch crystallinity and its correlation with double helix content: a combined XRD and NMR study, Biopolymers 89 (2008) 761–768, https://doi.org/ 10.1002/bip.21005.

[13] R. Thakur, P. Pristijono, C.J. Scarlett, M. Bowyer, S.P. Singh, Q.V. Vuong, Starch-based films: major factors affecting their properties, Int. J. Biol. Macromol. 132 (2019) 1079–1089, https://doi.org/10.1016/j.ijbiomac.2019.03.190.

[14] N. Laohakunjit, A. Noomhorm, Effect of plasticizers on mechanical and barrier properties of rice starch film, Starch-Stärke 56 (2004) 348–356, https://doi.org/ 10.1002/star.200300249.

[15] G.A. Duarte, M.C. Bezerra, S.H.P. Bettini, A.A. Lucas, Real-time monitoring of the starch cross-linking with citric acid by chemorheological analysis, Carbohydr. Polym. 311 (2023), 120733, https://doi.org/10.1016/j.carbpol.2023.120733.

[16] K. Zhang, T. Su, F. Cheng, Y. Lin, M. Zhou, P. Zhu, R. Li, D. Wu, Effect of sodium citrate/polyethylene glycol on plasticization and retrogradation of maize starch, Int. J. Biol. Macromol. 154 (2020) 1471–1477, https://doi.org/10.1016/j. ijbiomac.2019.11.028.

[17] M. Zdanowicz, C. Johansson, Mechanical and barrier properties of starch-based films plasticized with two- or three-component deep eutectic solvents, Carbohydr. Polym. 151 (2016) 103–112, https://doi.org/10.1016/j.carbpol.2016.05.061.

[18] D.S. Lai, A.F. Osman, S.A. Adnan, I. Ibrahim, M.N. Ahmad Salimi, A.A. Alrashdi, Effective aging inhibition of the thermoplastic corn starch films through the use of green hybrid filler, Polymers 14 (2022) 2567, https://doi.org/10.3390/ polym14132567.

[19] C.H. Kim, D.W. Kim, K.Y. Cho, The influence of PEG molecular weight on the structural changes of corn starch in a starch/PEG blend, Polym. Bull. 63 (2009) 91–99, https://doi.org/10.1007/s00289-009-0065-8.

[20] H. Xu, L. Chen, Z. Xu, D.J. McClements, H. Cheng, C. Qiu, J. Long, H. Ji, M. Meng, Z. Jin, Structure and properties of flexible starch-based double network composite films induced by dopamine self-polymerization, Carbohydr. Polym. 299 (2023), 120106, https://doi.org/10.1016/j.carbpol.2022.120106.

[21] C. Menzel, E. Olsson, T.S. Plivelic, R. Andersson, C. Johansson, R. Kuktaite, L. Janstrom, K. Koch, Molecular structure of citric acid cross-linked starch films, Carbohydr. Polym. 96 (2013) 270–276, https://doi.org/10.1016/j. carbpol.2013.03.044.

[22] J.L. Wang, F. Cheng, P.X. Zhu, Structure and properties of urea-plasticized starch films with different urea contents, Carbohydr. Polym. 101 (2014) 1109–1115, https://doi.org/10.1016/j.carbpol.2013.10.050.

[23] M. Baiardo, G. Frisoni, M. Scandola, M. Rimelen, D. Lips, K. Ruffieux, E. Wintermantel, Thermal and mechanical properties of plasticized poly (L-lactic acid), J. Appl. Polym. Sci. 90 (2003) 1731–1738, https://doi.org/10.1002/app.12549.

[24] J. Henise, B.R. Hearn, G.W. Ashley, D.V. Santi, Biodegradable tetra-PEG hydrogels as carriers for a releasable drug delivery system, Bioconjug. Chem. 26 (2015) 270–278, https://doi.org/10.1021/bc5005476.

[25] C.H. Kim, E.J. Choi, J.K. Park, Effect of PEG molecular weight on the tensile toughness of starch/PCL/PEG blends, J. Appl. Polym. Sci. 77 (2000) 2049–2056, https://doi.org/10.1002/1097-4628(20000829)77:9<2049::AID-APP22>3.0.CO;2-C.

[26] H. Long, J. Gu, J. Jiang, L. Guan, X. Lin, W. Zhang, C. Hu, Mechanically strong and biodegradable holocellulose films prepared from *Camellia oleifera* shells, Carbohydr. Polym. 299 (2023), 120189, https://doi.org/10.1016/j.carbpol.2022.120189.

[27] Y.A. Mehdi, M. Fizir, A. Itatahine, H. He, P. Dramou, Preparation of multifunctional PEG-graft-halloysite nanotubes for controlled drug release, tumor cell targeting, and bio-imaging, Colloids Surf. B 170 (2018) 322–329, https://doi.org/10.1016/j.colsurfb.2018.06.042.

[28] E. Olsson, M.S. Hedenqvist, C. Johansson, L. Järnström, Influence of citric acid and curing on moisture sorption, diffusion and permeability of starch films, Carbohydr. Polym. 94 (2013) 765–772, https://doi.org/10.1016/j.carbpol.2013.02.006.

[29] R. Ortega-Toro, S. Collazo-Bigliardi, P. Talens, A. Chiralt, Influence of citric acid on the properties and stability of starch-polycaprolactone based films, J. Appl. Polym. Sci. 133 (2016) 42220, https://doi.org/10.1002/app.42220.

[30] S.Z. Rogovina, K.V. Aleksanyan, A.A. Loginova, N.E. Ivanushkina, L.V. Vladimirov, E.V. Prut, A.A. Berlin, Influence of PEG on mechanical properties and biodegradability of composites based on PLA and starch, Starch-Stärke 70 (2018) 1700268, https://doi.org/10.1002/star.201700268.

[31] A.L. Da Róz, A.J.F. Carvalho, A. Gandini, A.A.S. Curvelo, The effect of plasticizers on thermoplastic starch compositions obtained by melt processing, Carbohydr. Polym. 63 (2006) 417–424, https://doi.org/10.1016/j.carbpol.2005.09.017.

[32] E. Piacenza, A. Presentato, R. Alduina, A. Scurria, M. Pagliaro, L. Albanese, F. Meneguzzo, R. Ciriminna, D.F. Chillura Martino, Cross-linked natural IntegroPectin films from Citrus biowaste with intrinsic antimicrobial activity, Cellulose 29 (2022) 5779–5802, https://doi.org/10.1007/s10570-022-04627-1.

[33] R.G. Alamo, J.A. Blanco, I. Carrilero, R. Fu, Measurement of the ^{13}C spin–lattice relaxation time of the non-crystalline regions of semicrystalline polymers by a cp MAS-based method, Polymer 43 (2002) 1857–1865, https://doi.org/10.1016/S0032-3861(01)00761-3.

[34] P. Conte, A. Piccolo, B. Van Lagen, P. Buurman, P.A. De Jager, Quantitative aspects of solid-state 13C-NMR spectra of humic substances from soils of volcanic systems, Geoderma 80 (1997) 327–338, https://doi.org/10.1016/S0016-7061(97)00058-X.

[35] P. Conte, R. Spaccini, A. Piccolo, State of the art of CPMAS ^{13}C-NMR spectroscopy applied to natural organic matter, Prog. Nucl. Magn. Reson. Spectrosc. 44 (2004) 215–223, https://doi.org/10.1016/j.pnmrs.2004.02.002.

[36] G. Landi, G.V. Spinelli, F. Zama, D. Chillura Martino, P. Conte, P. Lo Meo, V. Bortolotti, An automatic L_1-based regularization method for the analysis of FFC dispersion profiles with quadrupolar peaks, Appl. Math. Comput. 444 (2023), 127809, https://doi.org/10.1016/j.amc.2022.127809.

[37] P. Lo Meo, S. Terranova, A. Di Vincenzo, D.F. Chillura Martino, P. Conte, Heuristic algorithm for the analysis of fast field cycling (FFC) NMR dispersion curves, Anal. Chem. 93 (2021) 8553–8558, https://doi.org/10.1021/acs.analchem.1c01264.

[38] S. Mali, L.S. Sakanaka, F. Yamashita, M.V.E. Grossmann, Water sorption and mechanic properties of cassava starch films and their relation to plasticizing effect, Carbohydr. Polym. 60 (2005) 283–289, https://doi.org/10.1016/j.carbpol.2005.01.003.

[39] G. Velazquez de la Cruz, J.A. Torres, M.O. Martin-Polo, Temperature effect on the moisture sorption isotherms for methylcellulose and ethylcellulose films, J. Food Eng. 48 (2001) 91–94, https://doi.org/10.1016/S0260-8774(00)00143-6.

[40] M. Peleg, An empirical model for the description of moisture sorption curves, J. Food Sci. 53 (1988) 1216–1217.

[41] Y. Jiugao, W. Ning, M. Xiaofei, The effects of citric acid on the properties of thermoplastic starch plasticized by glycerol, Starch-Stärke 57 (2005) 494–504, https://doi.org/10.1002/star.200500423.

[42] A. Ounkaew, P. Kasemsiri, K. Kamwilaisak, K. Saengprachatanarug, W. Mongkolthanaruk, M. Souvanh, U. Pongsa, P. Chindaprasirt, Polyvinyl alcohol (PVA)/starch bioactive packaging film enriched with antioxidants from spent coffee ground and citric acid, J. Polym. Environ. 26 (2018) 3762–3772, https://doi.org/10.1007/s10924-018-1254-z.

[43] P.G. Seligra, C.M. Jaramillo, L. Famá, S. Goyanes, Biodegradable and non-retrogradable eco-films based on starch–glycerol with citric acid as crosslinking agent, Carbohydr. Polym. 138 (2016) 66–74, https://doi.org/10.1016/j.carbpol.2015.11.041.

[44] R. Shi, J. Bi, Z. Zhang, A. Zhu, D. Chen, X. Zhou, L. Zhang, W. Tian, The effect of citric acid on the structural properties and cytotoxicity of the polyvinyl alcohol/ starch films when molding at high temperature, Carbohydr. Polym. 74 (2008) 763–770, https://doi.org/10.1016/j.carbpol.2008.04.045.

[45] N. Reddy, Y. Yang, Citric acid cross-linking of starch films, Food Chem. 118 (2010) 702–711, https://doi.org/10.1016/j.foodchem.2009.05.050.

[46] A. Uliniuc, T. Hamaide, M. Popa, S. Bǎcǎiţǎ, Modified starch-based hydrogels cross-linked with citric acid and their use as drug delivery systems for levofloxacin, Soft Mater. 11 (2013) 483–493, https://doi.org/10.1080/1539445X.2012.710698.

[47] Y. Yamaguchi, Y. Okawa, K. Ninomiya, H. Kumagai, H. Kumagai, Evaluation and suppression of retrogradation of gelatinized rice starch, J. Nutr. Sci. Vitaminol. 65 (2019) S134–S138, https://doi.org/10.3177/jnsv.65.S134.

[48] C.G. Biliaderis, Chapter 8 - structural transitions and related physical properties of starch, in: J. BeMiller, R. Whistler (Eds.), Starch Chemistry and Technology, 3rd edn., Academic Press, Burlington (MA, USA), 2009, pp. 293–372, https://doi.org/10.1016/B978-0-12-746275-2.00008-2.

[49] C.K. Mouzakitis, V. Sereti, A. Matsakidou, K. Kotsiou, C.G. Biliaderis, A. Lazaridou, Physicochemical properties of zein-based edible films and coatings for extending wheat bread shelf life, Food Hydrocoll. 132 (2022), 107856, https://doi.org/10.1016/j.foodhyd.2022.107856.

[50] M. Tako, Y. Tamaki, T. Teruya, Y. Takeda, The principles of starch gelatinization and retrogradation, Food Nutr. Sci. 5 (2014) 42262, https://doi.org/10.4236/fns.2014.53035.

[51] S. Wang, C. Li, L. Copeland, Q. Niu, S. Wang, Starch retrogradation: a comprehensive review, Compr. Rev. Food Sci. Food Saf. 14 (2015) 568–585, https://doi.org/10.1111/1541-4337.12143.

[52] F.J. Warren, M.J. Gidley, B.M. Flanagan, Infrared spectroscopy as a tool to characterise starch ordered structure—a joint FTIR–ATR, NMR, XRD and DSC study, Carbohydr. Polym. 139 (2016) 35–42, https://doi.org/10.1016/j.carbpol.2015.11.066.

[53] M. Mathlouthi, J.L. Koenig, Vibrational spectra of carbohydrates, Adv. Carbohydr. Chem. Biochem. 44 (1987) 7–89, https://doi.org/10.1016/S0065-2318(08)60077-3.

[54] L. Chen, F. Ren, Z. Zhang, Q. Tong, M.M.A. Rashed, Effect of pullulan on the short-term and long-term retrogradation of rice starch, Carbohydr. Polym. 115 (2015) 415–421, https://doi.org/10.1016/j.carbpol.2014.09.006.

[55] S.I. Shin, C.J. Lee, M.J. Kim, S.J. Choi, H.J. Choi, Y. Kim, T.W. Moon, Structural characteristics of low-glycemic response rice starch produced by citric acid treatment, Carbohydr. Polym. 78 (2009) 588–595, https://doi.org/10.1016/j.carbpol.2009.05.017.

[56] Y. Huang, F. Meng, R. Liu, Y. Yu, W. Yu, Morphology and supramolecular structure characterization of cellulose isolated from heat-treated moso bamboo, Cellulose 26 (2019) 7067–7078, https://doi.org/10.1007/s10570-019-02614-7.

[57] O.S. Lawal, Starch hydroxyalkylation: Physicochemical properties and enzymatic digestibility of native and hydroxypropylated finger millet (*Eleusine coracana*) starch, Food Hydrocoll. 23 (2009) 415–425, https://doi.org/10.1016/j.foodhyd.2008.02.013.

[58] M.J. Gidley, S.M. Bociek, Molecular organization in starches: a carbon ^{13} CP/MAS NMR study, J. Am. Chem. Soc. 107 (1985) 7040–7044, https://doi.org/10.1021/ja00310a047.

[59] A. Poulhazan, A.A. Arnold, D.E. Warschawski, I. Marcotte, Unambiguous ex situ and in cell 2D 13C solid-state NMR characterization of starch and its constituents, Int. J. Mol. Sci. 19 (2018) 3817, https://doi.org/10.3390/ijms19123817.

[60] F. Ivanič, D. Jochec-Mošková, I. Janigová, I. Chodák, Physical properties of starch plasticized by a mixture of plasticizers, Eur. Polym. J. 93 (2017) 843–849, https://doi.org/10.1016/j.eurpolymj.2017.04.006.

[61] T.E. Motaung, M.L. Saladino, A.S. Luyt, D.F. Chillura Martino, The effect of silica nanoparticles on the morphology, mechanical properties and thermal degradation kinetics of polycarbonate, Compos. Sci. Technol. 73 (2012) 34–39, https://doi.org/10.1016/j.compscitech.2012.08.014.

[62] L. Tammaro, V. Vittoria, V. Bugatti, Dispersion of modified layered double hydroxides in poly (ethylene terephthalate) by High Energy Ball Milling for food packaging applications, Eur. Polym. J. 52 (2014) 172–180, https://doi.org/10.1016/j.eurpolymj.2014.01.001.

[63] Y. Ke, C. Long, Z. Qi, Crystallization, properties, and crystal and nanoscale morphology of PET–clay nanocomposites, J. Appl. Polym. Sci. 71 (1999) 1139–1146, https://doi.org/10.1002/(SICI)1097-4628(19990214)71:7<1139::AID-APP12>3.0.CO;2-E.

[64] C.I. Calcagno, C.M. Mariani, S.R. Teixeira, R.S. Mauler, The effect of organic modifier of the clay on morphology and crystallization properties of PET nanocomposites, Polymer 48 (2007) 966–974, https://doi.org/10.1016/j.polymer.2006.12.044.

[65] B.W. Chieng, N.A. Ibrahim, W.M.Z.W. Yunus, M.Z. Hussein, Plasticized poly (lactic acid) with low molecular weight poly (ethylene glycol): mechanical, thermal, and morphology properties, J. Appl. Polym. Sci. 130 (2013) 4576–4580, https://doi.org/10.1002/app.39742.

[66] J. Sievers, K. Sperlich, T. Stahnke, C. Kreiner, T. Eickner, H. Martin, R.F. Guthoff, M. Schunemann, S. Bohn, O. Stachs, Determination of hydrogel swelling factors by two established and a novel non-contact continuous method, J. Appl. Polym. Sci. 138 (2021) 50326, https://doi.org/10.1002/app.50326.

[67] P. Veiga-Santos, L.M. Oliveira, M.P. Cereda, A.R.P. Scamparini, Sucrose and inverted sugar as plasticizer. Effect on cassava starch–gelatin film mechanical properties, hydrophilicity and water activity, Food Chem. 103 (2007) 255–262, https://doi.org/10.1016/j.foodchem.2006.07.048.

[68] Y.H. Yun, S.D. Yoon, Effect of amylose contents of starches on physical properties and biodegradability of starch/PVA-blended films, Polym. Bull. 64 (2010) 553–568, https://doi.org/10.1007/s00289-009-0158-4.

[69] J.B.A. Da Silva, F.V. Pereira, J.I. Druzian, Cassava starch-based films plasticized with sucrose and inverted sugar and reinforced with cellulose nanocrystals, J. Food Sci. 77 (2012) N14–N19.

[70] L. Famá, A.M. Rojas, S. Goyanes, L. Gerschenson, Mechanical properties of tapioca-starch edible films containing sorbates, LWT 38 (2005) 631–639, https://doi.org/10.1016/j.lwt.2004.07.024.

[71] R.K. Basha, K.Y. Leong, S.H. Othman, R.A. Talib, M.N. Naim, N.Z.N. Hasnan, N. S. Azmi, Sorption characteristic of starch-based film, Food Res. 5 (2021) 193–200, https://doi.org/10.26656/fr.2017.5(S1).056.

[72] A. Lindstrom, M. Hakkarainen, Migration resistant polymeric plasticizer for poly (vinylchloride), J. Appl. Polym. Sci. 104 (2007) 2458–2467, https://doi.org/10.1002/app.24777.

[73] C.E. Chinma, C.C. Ariahu, J.S. Alakali, Effect of temperature and relative humidity on the water vapour permeability and mechanical properties of cassava starch and soy protein concentrate based edible films, J. Food Sci. Technol. 52 (2015) 2380–2386, https://doi.org/10.1007/s13197-013-1227-0.